Available online at www.sciencedirect.com
SCIENCE DIRECT®
Physica B 370 (2005) 200–214
PHYSICA B
www.elsevier.com/locate/physb

Tight-binding and evolutionary search approach for nanoscale CoRh alloys

A. Díaz-Ortiz[a,*], F. Aguilera-Granja[b], K. Michaelian[c], E.O. Berlanga-Ramírez[b], J.M. Montejano-Carrizales[b], A. Vega[d]

[a]*Texas Materials Institute, The University of Texas at Austin, 78712 Austin, TX, USA*
[b]*Instituto de Física, Universidad Autónoma de San Luis Potosí, 78000 San Luis Potosí, S.L.P., Mexico*
[c]*Instituto de Física, Universidad Nacional Autónoma de México, 20-364, 01000 México, D.F., Mexico*
[d]*Departamento de Física Teórica, Atómica y Óptica, Universidad de Valladolid, E-47005 Valladolid, Spain*

Received 22 April 2005; received in revised form 28 September 2005; accepted 28 September 2005

Abstract

The dependence of the structural and magnetic properties of Co–Rh alloys at the nanoscale was investigated by exhaustively searching the minimum energy via a symbiotic algorithm on a Gupta potential for particle sizes of 13, 19, and 23 atoms. An unrestricted spd tight-binding Hamiltonian was then used to model the electronic properties. Our results underscore the importance of determining both the geometrical and the chemical configuration. A central result points toward a surface segregation that *qualitatively* and *quantitatively* depends on system size, with size effects dominating the surface segregation for small Co–Rh clusters (Rh atoms preferentially occupy surface sites), whereas surface energy dictates the segregation for large Co–Rh nanoparticles (Co segregates to the surface). This might have important consequences for heterogeneous catalysis, where the catalytic activity strongly depends on surface composition.

PACS: 36.40.Cg; 61.46.+w; 73.22.−f; 75.50.Tt; 75.75.+a

Keywords: Nanostructures; Magnetism; Structure

1. Introduction

Alloying is one of the most important and fundamental mechanisms known to modify material's behavior. By combining two or more elements, one aims to impart (or enhance) a desired set of properties of the individual

*Corresponding author. Tel.: +1 512 4716709; fax: +1 512 4717681.
E-mail address: ado@mail.utexas.edu (A. Díaz-Ortiz).

0921-4526/$ - see front matter © 2005 Elsevier B.V. All rights reserved.
doi:10.1016/j.physb.2005.09.012

components to the resulting alloy. By alloying, it is possible to increase the hardness above that of the individual components, e.g., in Cu–Zn alloys [1]; to avoid corrosion, as in stainless steels [2]; or to increase the magnetic moment to the largest value in a binary compound as in the case of Fe–Co alloys [3]. Also by allowing, it is possible to induce a magnetic moment in an otherwise nonmagnetic ion, e.g., Co–Rh alloys [4].

A different way to modify material's properties is by controlling its size. Low-dimensional nanoscale systems offer an ideal arena to explore the interdependence between finite size and surface effects [5]. Because of the technological implications, as well as for their importance in understanding fundamental phenomena, particular attention has been devoted to transition-metal clusters. Using a Stern–Gerlach deflection apparatus coupled with a laser vaporization cluster source and time-of-flight mass spectroscopy, several groups have measured the magnetic moment of 3d transition-metal clusters. Their results showed that the magnetic moment per atom is greatly enhanced with respect to the bulk value [6–10]. In such ferromagnetic systems, the reduction of the dimensionality leads to a decrease in the bandwidth thus promoting electronic localization. However, this mechanism also applies to nonmagnetic 4d transition-metal clusters. It was first theoretically predicted [11,12] and later experimentally confirmed [13,14], that Rh, Ru, and Pd nanoparticles presented nonvanishing magnetic moments.

The cases of Rh and Pd metals deserve some special attention because of their subtle magnetic properties, i.e., they are "almost" magnetic even at equilibrium volumes. First-principles calculations of the spin-polarized electronic structure of bulk transition metals showed that, upon a hydrostatic expansion, the magnetic moment approached the atomic limit from below, with the exception of Rh and Pd where the magnetic moment exceeded the Hund's rule and approached the atomic limit from above [15]. Further investigations on Rh and Pd nanoparticles, either deposited on noble metal substrates [16,17], neutral and anionic clusters [18–22], monoatomic chains [23], or in the form of contacts and nanowires [24], have shown that they possess subtle magnetic properties, where Hund's rule presence strongly depends on the details of the nanoparticle structure.

Very recently, these two approaches of modifying material's properties, i.e., alloying and size control, have been combined to produce nanoscale bimetallic particles with new and interesting magnetic, optical and catalytic properties [25]. Metal nanoparticles can be prepared by physical or chemical methods. The physical methods consist, in general, of subdividing bulk precursors to nanoparticles. Chemical methods, on the other hand, start from the reduction of metal ions to metal atoms, followed by controlled aggregation of atoms. From the view point of mass production, where achieving uniformity is an all-important aspect, chemical methods are more important and effective than the physical procedure for producing metal nanoparticles.

Nonsupported metal nanoparticles have several advantages over the supported ones: the intrinsic properties of the nanoparticles can be elucidated without the particle–substrate interaction. Also, a more uniform particle size distribution can be attained than in the supported cases. Ligants or polymers, especially solvent-soluble polymers either natural or synthetic, with affinity for metals are often used as stabilizers of metal nanoparticles. Polymers also control the aggregation process of metal atoms in solution. It has been shown that mono [26–29] and bimetallic [30–33] transition-metal nanoparticles stabilized by poly(vinylpyrrolidone) (PVP) present a narrow size distribution and virtually no effect from the polymer–particle interaction. Co-rich Co–Pt [30], Co–Rh [31–33], and Co–Ru [33], metallic nanoparticles embedded in PVP show nonperiodical polytetrahedral structure, whereas 4d transition-metal-rich particles display the bulk structure of the heavy transition metal, i.e., face-centered cubic (FCC) in the case of Pt and Rh, hexagonal closed-packed (HCP) in the case of Ru.

Regarding the magnetic properties of chemically produced bimetallic nanoparticles, the most interesting behavior has been observed in Co–Rh nanoparticles. Zitoun and collaborators [31–33] have synthesized bimetallic particles of Co and Rh by the simultaneous decomposition of two

organometallic precursors in an organic solution of PVP. The average size of the nanoparticles was between 1.7 and 4.1 nm with stoichiometries ranging between $Co_{0.47}Rh_{0.53}$ and $Co_{0.55}Rh_{0.45}$. Magnetic measurements on such samples revealed a decrease of the coercive field with size but a simultaneous increase of the anisotropy field. Surprisingly enough, at 30 T the average magnetic moment per CoRh [34] unit is $2.38\mu_B$ for the smaller sized CoRh nanoparticles, i.e., twice of the corresponding bulk (theoretical) value [35]. The enhancement of the magnetic moment per atom cannot be attributed solely to an enhancement of the Co magnetic moment, even if one assumes some Co atoms segregated at the surface or considers the orbital contribution to the magnetic moment. This suggests a large Rh contribution to the magnetism of nanoscale Co–Rh particles. Chemical ordering might also be playing an important role in determining the magnetic properties of such Co–Rh particles. However, even though their wide-angle X-ray scattering (WAXS) measurements are in favor of an alloyed structure rather than core-shell particles, the overall results of Zitoun et al., [31–33] do not permit to definitively distinguish between phase-separated and homogeneously alloyed Co–Rh nanoparticles.

The above scenario has prompted some theoretical investigations on nanoscale Co–Rh particles. A first-principles investigation on very small Co–Rh clusters revealed that, for a given cluster, the average magnetic moment increased with the number of Co atoms [36]. In such study, it was also found an enhancement of the average magnetic moment per atom, in agreement with experiment [31–33]. However, due to the rather small cluster sizes (up to four atoms) considered in Ref. [36], the question of alloyed vs core-shell Co–Rh particles was not investigated. This is an important point that deserves to be emphasized: in order to make contact with experiments of Zitoun and coworkers [31–33], it is necessary to consider particles with several hundreds of atoms and, consequently, computational tools capable of handling such number of atoms. The electronic structure of the bimetallic nanoscale particles can be fairly well represented in a tight-binding scheme, being the aspect of the geometry optimization of the nanoparticles, the major obstacle to overcome by theoreticians. In a recent paper, we have investigated the role of the structure and chemical ordering on the magnetism on Co–Rh particles (with as many as 115 atoms), in selected structures that were locally optimized [37]. Our results showed great consistency with the experimental measurements, in that magnetization of the uniformly alloyed Co–Rh nanoparticles is virtually indistinguishable from the phase-separated (core-shell) structured particles; in that we found an enhancement of the average magnetic moment per atom, but also an induced magnetic moment at Rh sites is found [37].

Assuming a given structure (even with an educated guess) and then locally optimizing it, in order to investigate the magnetism on Co–Rh nanoparticles has, evidently, certain disadvantages. The most evident is that the "real" structure and configurational ordering are still unknown—although the alloyed vs core-shell chemical order of the Co–Rh particle can be studied with the prototype structures. An investigation of nanoscale Co–Rh particles, where global searches for the most stable structure are carried out, is important because it is well known that geometry plays an all-important role determining the physical and chemical properties of nanoparticles. On the other hand, it is also important to compare semiempirical schemes (as the one advanced in Ref. [37]) that have proved to be successful in describing the structure and magnetism of "large" Co–Rh nanoparticles, with the more accurate, first-principles total-energy calculations in "very small" Co–Rh clusters [36], so to verify to what extent the observed trends and behaviors in one extreme of the size range are still valid in the other. We aim to fill such gaps with this paper.

A global-search algorithm, based on a symbiotic variant of the genetic algorithm, was used to perform exhaustive searches for the ground-state structure (along with an extensive set of low-energy isomers) of Co–Rh nanoparticles. Even with the use of a Gupta potential to describe the potential energy surface, the practical size limit is reached very soon for the bimetallic clusters ($\sim$40 atoms with current computational capabilities). This is because the number of nondegenerate

permutational isomers at this size for equal numbers of Co and Rh atoms is $40!/20!20! = 1.38 \times 10^{11}$ (symmetries reduce this number somewhat).We focused on Co–Rh nanoparticles of 13, 19, and 23 atoms with an stoichiometry as close as possible to the equiatomic composition. Due to the finite size of the system, it is not always possible to achieve 50/50 Co–Rh nanoparticles, and in most cases, small deviations from stoichiometry are found, e.g., for 13-atom nanoparticles we have investigated both Co_6Rh_7 and Co_7Rh_6. This, on the other hand, has provided us with the opportunity to test the magnetic and structural properties against small variations in composition (see, for example, the paper of Zitoun and coworkers [31–33]).

We have organized the rest of the paper as follows. In Section 2, we review the computational tools used in this study. The results obtained from applying the combined tight-binding and evolutionary search approached to Co and Rh nanoparticles are discussed in Section 3, followed by the conclusions in Section 5. Comparison with experiments and previous theoretical work is done when applicable.

2. Computational methods

2.1. The symbiotic algorithm and the Gupta potential

Genetic algorithms [38] are inspired by the Darwinian evolution processes, where the search of a set of variables that optimizes a fitness function, e.g. the energy, is performed over populations (ensembles) rather than on single individuals. For such reason, the optimization process can be considered an evolutionary process on successive generations. The fitness of every generation is evaluated at each step of the optimization procedure. The fittest solutions are then chosen as the ''parents'' of the next generation. Broadly speaking, a generation can evolve through three main processes: crossover, mutation, and selection [39]. In recent years, genetic algorithms have proved to be the tool of choice for global geometry optimization in nanoparticles (see, for example, Refs. [40–44], and references therein).

We have employed a symbiotic algorithm [44], an efficient variant of the genetic algorithm, to find the global minimum structure for Co_pRh_q nanoparticles with $p \sim q \leqslant 12$. The symbiotic algorithm profits from the fact that interactions in metallic clusters are short ranged, i.e., nearest neighbors atoms are tightly bound. Owing to the fact that bimetallic nanoparticles possess energy landscapes having many local minima, our approach uses a global genetic algorithm with stochastic moves on the potential energy surface (to avoid entrapment in high-energy local minima), combined with a conjugate gradient local relaxation (once the global part has reached the attraction basins of the lowest-energy minima).

The symbiotic algorithm begins by generating a random initial configuration of the cluster atomic coordinates within a sphere large enough to allow for all possible structural conformations. A spherical cell of smaller radius is defined so as to include a small number of atoms whose coordinates are then optimized by a global genetic algorithm. The rest of the atoms, i.e., those sitting between the two spheres, remain fixed yet contributing to the cluster energetics. At this point, a symbiosis is formed between the cell and the rest of the nanoparticle atoms, updating atomic coordinates if the fitness function is indeed optimized. The process is then repeated, every time using a different atom to center the spherical cell. Gradually, the size of the cell is increased until the whole cluster fits within a cell. When the binding energy of the cluster no longer increases from one generation to the next, for a certain specified number of generations, the genetic part is stopped and the whole nanoparticle is then locally optimized by applying the conjugate gradient technique. For each cluster size, we carried out $\sim 10^5$ symbiotic optimizations, each optimization beginning from a distinct random initial configuration.

The symbiotic algorithm just described operates on the potential energy surface of the n-body Gupta potential [45] which is based on the second moment approximation to the density of states in a tight-binding model (second term in the right-hand side of Eq. (1)). The repulsive part of the potential,

on the other hand, is described by a Born–Meyer term [first term in Eq. (1)]

$$V = \sum_{i=1}^{n} \left[A \sum_{j(\neq i)=1}^{n} \exp[-p(r_{ij}/r_{0n} - 1)] - \left(\xi^2 \sum_{j(\neq i)=1}^{n} \exp[-2q(r_{ij}/r_{0n} - 1)] \right)^{1/2} \right], \quad (1)$$

where A, ξ, p and q are fitted to the experimental values of the bulk cohesive energy, lattice parameters and elastic constants [46], and the r_{0n} were taken as the bulk nearest-neighbor distances. For the hetero-interactions, an arithmetic mean was taken for the parameters related to the distance, p, q, and r_{0n}, while a geometric mean was taken for parameters associated to the strength, A and ξ. The values of the parameters used are given in Table 1.

2.2. Electronic structure

Once the Co–Rh nanoparticles structures were determined as explained above, their electronic structure was calculated by solving a spd tight-binding Hamiltonian in the unrestricted Hartree–Fock approximation. In its second quantization form, the Hamiltonian can be written as

$$H = \sum_{i,\alpha,\sigma} \varepsilon_{i\alpha\sigma} n_{i\alpha\sigma} + \sum_{\substack{i,\alpha,\sigma \\ i \neq j}} t_{ij}^{\alpha\beta} c_{i\alpha\sigma}^{\dagger} c_{j\beta\sigma}, \quad (2)$$

Table 1
Parameters used in the Gupta potential [Eq. (1)] as applied in this work

	A (eV)	ξ (eV)	p	q	r_{0n} (Å)
Co–Co	0.0955	1.488	11.604	2.286	2.506
Rh–Rh	0.0629	1.660	18.450	1.867	2.690
Co–Rh	0.0773	1.572	15.027	2.077	2.598

A, ξ, p and q were fitted to the experimental values of the bulk cohesive energy, lattice parameters and elastic constants [46], and the r_{0n} were taken as the bulk nearest-neighbor distances. For the hetero-interactions, an arithmetic mean was taken for the parameters related to the distance, p, q and r_{0n}, while a geometric mean was taken for parameters related to the strength, A and ξ.

where the $t_{ij}^{\alpha\beta}$ stands for the hopping integral of electrons with spin σ between orbitals α and β at sites i and j, respectively. The density of electrons (the number operator) in the α orbital with spin σ located at site i is expressed in terms of the creation and annihilation operators, respectively, as $n_{i\alpha\sigma} = c_{i\alpha\sigma}^{\dagger} c_{i\alpha\sigma}$. The diagonal elements $\varepsilon_{i\alpha\sigma}$ include the electronic correlations and the dependency on the spin (see below).

We have solved Hamiltonian (2) in a self-consistent way, including hopping integrals up to second neighbors and assuming such hopping matrix elements to be spin independent. The chemical dependence of the $t_{ij}^{\alpha\beta}$'s was considered as follows: for the hopping between the same element (Co or Rh), two-center integrals reproducing the metal band structure were used along with the Slater–Koster approximation [47]. For the hopping between Co and Rh atoms, we have used the geometric average of the homoatomic hopping integrals, except for the two-center $pp\pi$ parameter between second neighbors, where an arithmetic mean was used—the parametrization used in Ref. [47] rendered a different sign in the case of Co and Rh.

The changes of the hopping integrals, reflecting in turn the deviation of the interatomic distances from their bulk values, were considered via a power law of the type $(r_0/r_{ij})^{l+l'+1}$. Here r_0 represents the bulk distance, between first or second neighbors, with l and l' standing for the orbital angular momenta of the electronic states involved in the process [48].

The first term on the right-hand side of Eq. (2) brings, on the one hand, the spin dependence of the Hamiltonian and, on the other, the electronic correlations (in the mean-field approximation) via a correction of the energy levels of the form

$$\varepsilon_{i\alpha\sigma} = \varepsilon_{i\alpha}^{0} + \frac{1}{2} z_{\sigma} \sum_{\beta} J_{i\alpha\beta} \mu_{i\beta} + \Omega_{i\alpha}, \quad (3)$$

with the bare energy of orbital α at site i denoted by $\varepsilon_{i\alpha}^{0}$ and the exchange integrals represented by $J_{i\alpha\beta}$. The change in sign of the second term on the right-hand side of Eq. (3) when switching from spin-up to spin-down is accounted for by the sign function $z_{\sigma} = \pm 1$, respectively. The spin

polarization of the sp band, due to hybridization with the d states, is negligible as compared with the dominant d band polarization. Thus, in our treatment of the spin-dependent part of Hamiltonian (2), we have only considered exchange integrals for the d electrons. In what follows, we have taken the exchange integral associated with Co atoms equal to 1.44 eV, in order to reproduce the Co bulk magnetic moment, without orbital contribution, of $1.59\mu_B$ (Ref. [49]). For Rh, on the other hand, we have fitted the exchange integral to the magnetic properties of icosahedral Rh_{13} and Rh_{19} clusters [18], because FCC Rh is nonmagnetic in the bulk. The obtained values $J_d(Rh) = 0.40\,eV$ and $J_d(Co) = 1.44\,eV$ have proven to accurately describe the magnetic moment of pure Co (Ref. [50]) and pure Rh clusters [21,22].

In our model, the local electronic occupation is fixed by linearly interpolating between the atom and the metal occupations according to the coordination at site i. The self-consistent potential $\Omega_{i\alpha}$, last term in Eq. (3), assures the local electronic occupation. Note that $\Omega_{i\alpha}$ has both an orbital and a site dependence. In all calculations, we have used the ground-state electronic configurations for the isolated atoms, i.e., Co = [Ar] $3d^7$ $4s^2$ and Rh = [Kr] $4d^8$ 5s. The metal electronic occupations, on the other hand, are those given in Ref. [47]: 0.64 (0.60), 0.34 (0.41), and 8.02 (7.99) for the s, p, and d electrons of Co (Rh), respectively.

3. Results

We have applied the computational methods described in Section 2 to nanoscale Co–Rh bimetallic particles of 13, 19, and 23 atoms. As described in the previous sections, we performed an exhaustive search for the minimum energy structure *and* chemical configuration for each cluster size and stoichiometry. Due to the finite size of the systems achieving an ideal 50/50 atomic distribution is not always possible. In the case of 13-atom nanoparticles, we searched the structural and configurational spaces for the following compositions Co_6Rh_7 and Co_7Rh_6. The results for the minimum and low-lying energy structures are shown in Fig. 1. It is interesting, although not completely unexpected, that both Co_6Rh_7 and Co_7Rh_6 ground-state structures have icosahedral symmetry [Figs. 1(a) and (d)], as well as the low-lying energy structures [Figs. 1(b)–(c) and (e)–(f), respectively], denoted here as iso01-Co_mRh_n and iso02-Co_mRh_n with $m, n = 6, 7$.

The atomic configuration depends sensitively on stoichiometry, as evidenced by the ground-state structures for Co_6Rh_7 [Fig. 1(a)] and Co_7Rh_6 [Fig. 1(d)], where for the latter a layered structure is found whereas for the former a slightly more "mixed" atomic distribution is obtained. For either stoichiometry, the low-lying energy structures are more "disordered" than the ground-state structures. This brings the important point of how to quantify the degree of atomic ordering in a bimetallic nanoparticle. Contrary to what happens in macroscopic systems, where periodicity allows for the definition of long- and short-range order parameters, based on symmetry considerations [51], in the nanoscale, however, due to the finite size of the system, such arguments are not fully applicable. To the best of the authors' knowledge, a consensus on how to describe the degree or ordering in bimetallic nanoparticles has not yet been achieved.

An order parameter for nanoscale bimetallic alloys should have the following (desirable) characteristics. First, it should be positive when phase separation (segregation) is present, pass by zero when completely disordered, and become negative otherwise (see Fig. 2). The following order parameter σ has the above properties:

$$\sigma = \frac{N_{Co-Co} + N_{Rh-Rh} - N_{Co-Rh}}{N_{Co-Co} + N_{Rh-Rh} + N_{Co-Rh}}, \tag{4}$$

where N_{ij} (with i,j = Co, Rh) is the number of nearest-neighbors i–j bonds. An order parameter of this sort has proven to be useful in the description of the short-range order in bulk binary alloys and surfaces thereof [51]. We have collected the value of σ together with some other geometrical parameters for the 13-atom Co–Rh nanoparticles (average size ~5.3 Å) in Table 2. As usual in transition-metal clusters, the interatomic distances are shortened with respect to bulk by about 5%.

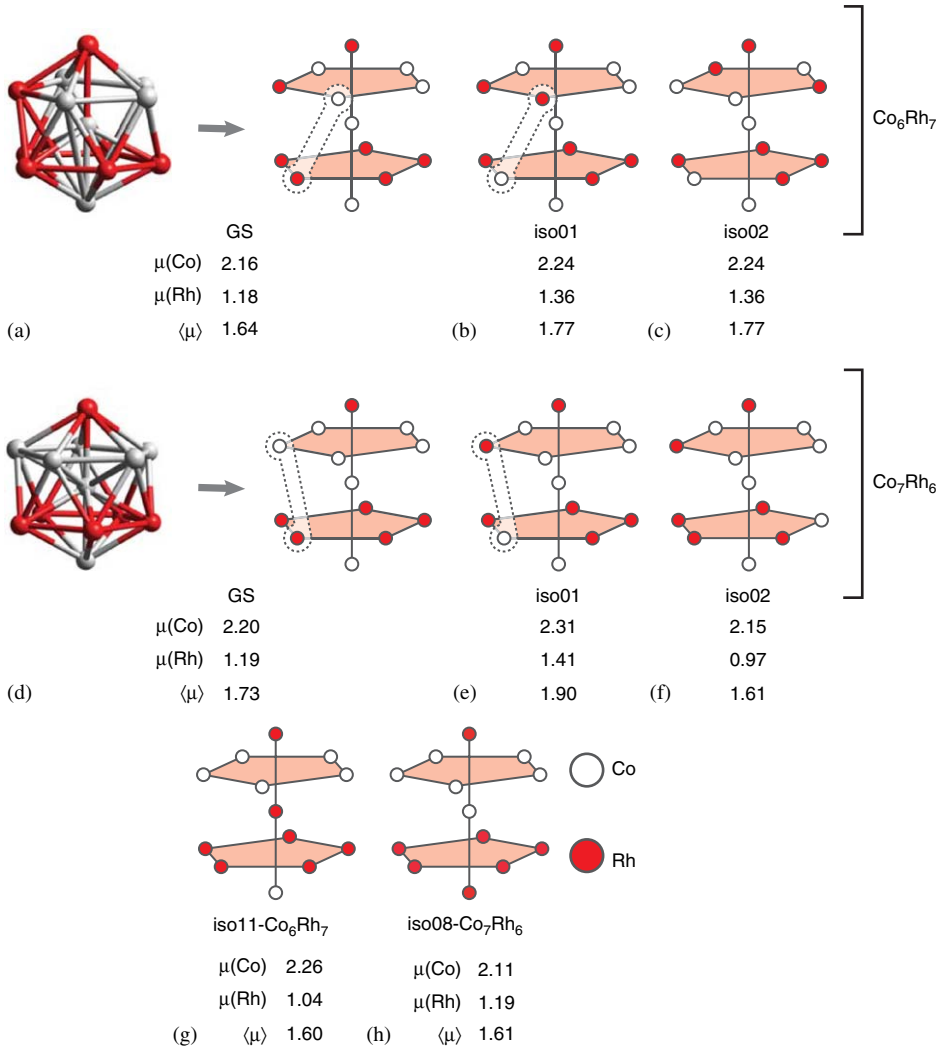

Fig. 1. (color on-line). Schematic representation of the ground-state and low-lying energy structures for 13-atom bimetallic Co–Rh nanoparticles, as obtained by our symbiotic algorithm based on a Gupta potential. All electronic properties were calculated via an spd unrestricted tight-binding Hamiltonian. The different averaged values for the magnetic moments (in Bohr magnetons) are reported in each case, e.g., μ(Co) stands for averaged value of the magnetic moment of all Co atoms. Observe that (g) and (h) indicate results for high symmetry configurations of Co_6Rh_7 nanoparticles that are isomers 11 and 8 in energy from the ground-state. See the text for further details.

The magnetic properties of the Co–Rh clusters are sensitive to the degree of ordering present in the system. For example, in the case of Co_mRh_n $(m,n=6,7)$ nanoparticles, the magnetic moment increases from the ground-state to the low-lying isomers. The Co_6Rh_7 average magnetic moment increases from $1.64\mu_B$ to $1.77\mu_B$ from the ground-state to the first isomer (iso01) just by exchanging two atoms between the five-membered rings [shadowed in Figs. 1(a)–(b)], in the same way that the average nanoparticle's magnetic moment of Co_7Rh_6 increases from $1.73\mu_B$ to $1.90\mu_B$ by the exact same mechanism (see Fig. 1). Interestingly enough, the value of the order parameter σ is the same for both the ground-state and the iso01 structures. Increasing the cobalt content increases

the value of the average magnetic moment in the nanoparticle, cf., the magnetic moment for Co_6Rh_7 and Co_7Rh_6 in Fig. 1.

For a 13-atom icosahedron, where 12 out of 13 atoms are at the surface, it is difficult to separate surface from finite-size effects and their impact on the magnetic properties. However, comparing the ground-state configuration between Co_6Rh_7 [Fig. 1(a)] and Co_7Rh_6 [Fig. 1(d)], tells us about the effect of layered vs mixed atomic arrangements, giving an indication of the surface segregation trends. Increasing the Co concentration in 1/13 means that one Rh atom has been replaced with a Co atom in the Co_6Rh_7 cluster. According to our results, the atomic substitution does not occur randomly, but in a way that made the Co_7Rh_6 ground-state a layered structure. Moreover, both Co_6Rh_7 and Co_7Rh_6 have a Co core atom in the ground-state and the first low-lying isomers, indicating that for small ($N = 13$) Co–Rh nanoparticles, Rh seems to segregate to the surface.

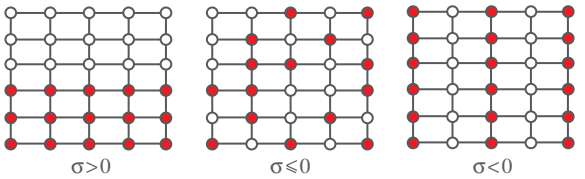

Fig. 2. (color on-line). Schematic representation of segregated, disordered, and layered bimetallic nanostructures, along with their corresponding value of the order parameter σ [defined in Eq. (4)]. Different colors represent different atomic species.

However, any physico-chemical tendency observed in very small clusters should be taken with caution, since it is well known that cluster properties are highly dependent on cluster size. This was corroborated for the bimetallic 19-atom Co_mRh_n with $m, n = 9$, 10 systems our symbiotic algorithm predicted double icosahedra for either composition as the ground-state and low-lying isomeric structures (Fig. 3). It is useful to point out some of the geometrical features characteristic of the Co–Rh 19-atom nanoparticles. First, and highly notorious, is the fact that all structures depicted in Fig. 3 have a Co atoms at the icosahedral axis, thus reinforcing the above idea of that Rh segregates to the surface. This characteristic is not limited to very first isomers. In fact, a $Co_{10}Rh_9$ isomer with an icosahedral axis made of exclusively Rh atoms was found to be isomer number 2537 in energy with respect to the ground-state [see Fig. 3(g)]. A second important motif, besides the Co icosahedral axis, is a central all-Rh pentagonal plane perpendicular to the latter axis, for all ground-state and low-lying isomers, irrespective of the composition. The energy penalty of having a Co_9Rh_{10} cluster with a central all-Co pentagonal plane, sets such isomer in position 1043 with respect to the ground-state [see Fig. 3(h)]. Third, in both the Co_9Rh_{10} and $Co_{10}Rh_9$ nanoparticles, the first low-lying isomer is related to the ground-state structure by a rotation of the basal pentagon around the icosahedral axis (indicated in Fig. 3 by a rounded rectangle) by $2\pi/5$ (clockwise) and $4\pi/5$ (counter-clockwise), respectively [52].

Table 2
Geometric characteristics of 13-atom Co–Rh nanoparticles

Iso	N_{Co-Co}	N_{Rh-Rh}	N_{Co-Rh}	D_{Rh-Rh}	D_{Co-Rh}	σ
GS-Co_6Rh_7	8	8	26	0.992	0.956	−0.238
01	8	8	26	0.992	0.956	−0.238
02	9	9	24	0.993	0.955	−0.143
GS-Co_7Rh_6	11	5	26	0.991	0.955	−0.238
01	11	5	26	0.991	0.955	−0.238
02	12	6	24	0.994	0.955	−0.143

The Co–Co nearest-neighbor bond length (D_{Co-Co}) remained constant for the GS and the first two low-lying isomers at 0.901 for Co_6Rh_7 and at 0.904 for Co_7Rh_6. The nanoparticle's average bond length was 0.952 and 0.946 for Co_6Rh_7 and Co_7Rh_6, respectively. The number of bond formed between the A and B atomic species is denoted by N_{A-B}. The associated average bond length is D_{A-B}. The total number of bonds is 42. All lengths are in units of bulk Rh–Rh bond length (2.69 Å).

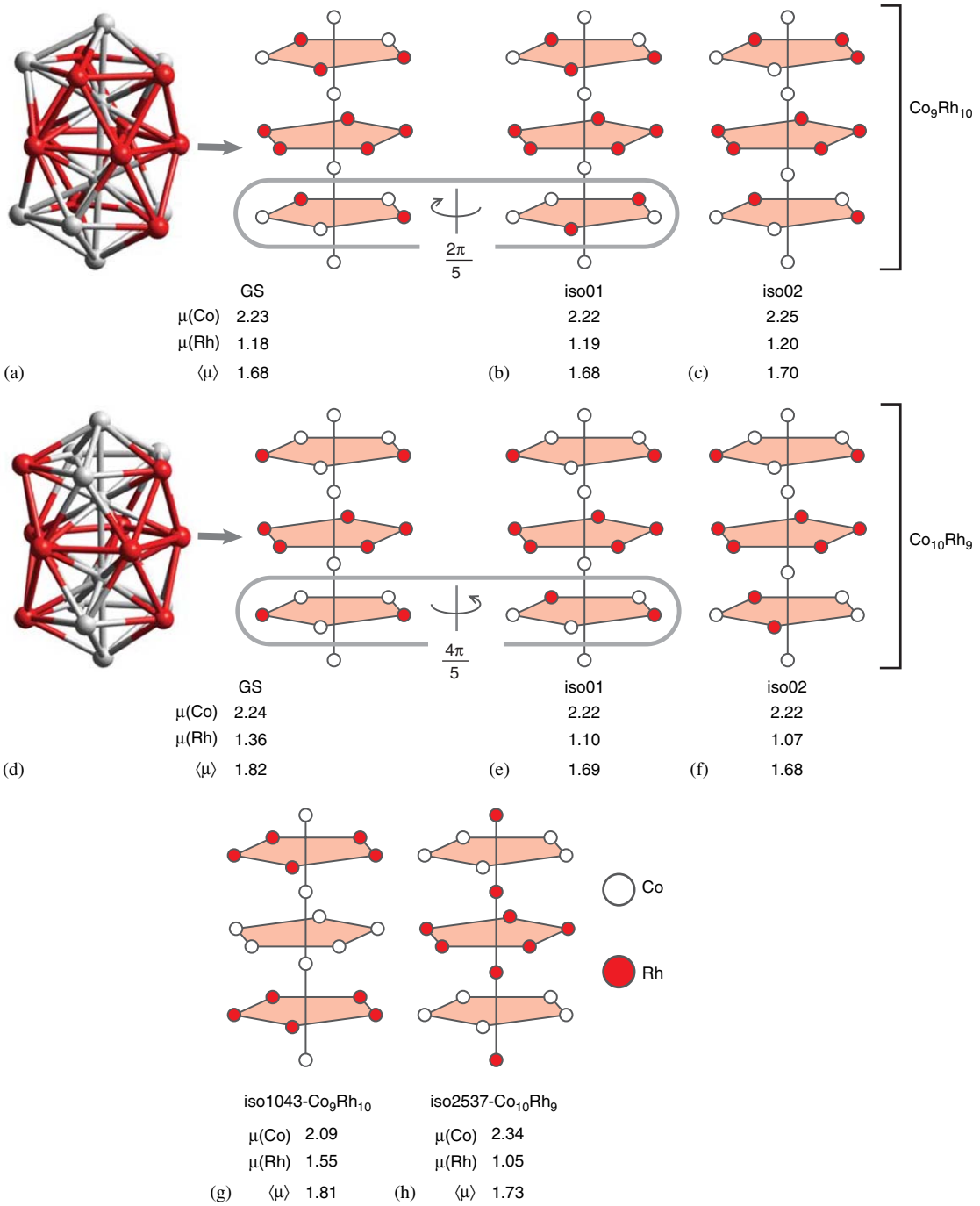

Fig. 3. (color on-line). Schematic representation of the ground-state and low-lying energy structures for 19-atom bimetallic Co–Rh nanoparticles, as obtained by our symbiotic algorithm based on a Gupta potential. All electronic properties were calculated via an spd unrestricted tight-binding Hamiltonian. The different averaged values for the magnetic moments (in Bohr magnetons) are reported in each case, e.g., μ(Co) stands for averaged value of the magnetic moment of all Co atoms. The rounded rectangles joining (a) with (b) and (d) with (e) are meant to emphasize that such structures are related via a rotation of the basal five-membered ring. The angle and direction of rotation are indicated in each case. Observe that (g) and (h) indicate results for high symmetry configurations of Co_9Rh_{10} and $Co_{10}Rh_9$ nanoparticles, isomers 1043 and 2537 in energy from the ground-state. See the text for further details.

Table 3
Geometric characteristics of 19-atom Co–Rh nanoparticles

Iso	N_{Co-Co}	N_{Rh-Rh}	N_{Co-Rh}	D_{Rh-Rh}	D_{Co-Rh}	σ
GS-Co_9Rh_{10}	14	16	38	1.000	0.958	−0.118
01	14	16	38	0.999	0.958	−0.118
02	15	17	36	1.000	0.958	−0.059
GS-$Co_{10}Rh_9$	13	15	40	0.994	0.954	−0.176
01	13	15	40	0.994	0.954	−0.176
02	14	16	38	0.993	0.954	−0.118

The Co–Co nearest-neighbor bond length (D_{Co-Co}) remained constant for the GS and the first two low-lying isomers at 0.900 for Co_9Rh_{10} and at 0.896 for $Co_{10}Rh_9$. The nanoparticle's average bond lengths were 0.956 and 0.952 for Co_9Rh_{10} and $Co_{10}Rh_9$, respectively. The number of bond formed between the A and B atomic species is denoted by N_{A-B}. The associated average bond length is D_{A-B}. The total number of bonds is 68. All lengths are in units of bulk Rh–Rh bond length (2.69 Å).

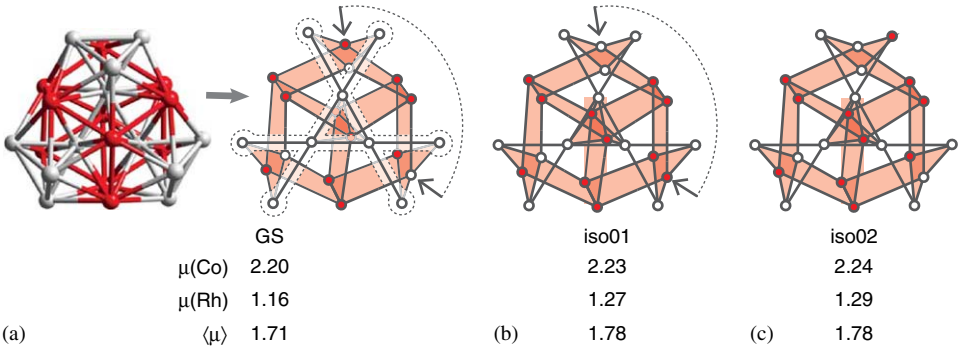

Fig. 4. (color on-line). Schematic representation of the ground-state and low-lying energy structures for 23-atom bimetallic $Co_{12}Rh_{11}$ nanoparticles, as obtained by our symbiotic algorithm based on a Gupta potential. All electronic properties were calculated via an spd unrestricted tight-binding Hamiltonian. The different averaged values for the magnetic moments (in Bohr magnetons) are reported in each case, e.g., μ(Co) stands for averaged value of the magnetic moment of all Co atoms. In (a) we have shadowed the main icosahedral axes. The ground-state and the first low-lying isomer are related by the interchange of two atoms (marked with arrows). See the text for further details.

This is a quite interesting observation, especially under the light shed by the results obtained for 13-atom Co–Rh nanoparticles, where the first low-lying isomer was related to the ground-state by an interchange of two atoms between the pentagons, independently of the composition (see Fig. 1). Table 3 collects some geometrical properties of these 19-atom icosahedral Co–Rh nanoparticles (average size ~7.9 Å along the main axis).

Our symbiotic algorithm allowed us to explore the ground-state and low-lying configurations of 23-atom Co–Rh nanoparticles. Here there are $23!/12!\,11! = 1.62 \times 10^7$ possible distinct permutational isomers for every geometrical isomer. Due to these numerical difficulties, we have only analyzed the case of $Co_{12}Rh_{11}$ nanoparticles, especially because the increase of Co concentration reflects in a simple increase of the cluster average magnetic moment without any further subtleties. Our calculations for the 23-atom clusters, enable us to check the validity of the extrapolation of the previous geometrical and chemical trends, observed in 13-atom and 19-atom Co–Rh nanoparticles. Fig. 4 contains the resulting geometric structures and configurational permutations obtained for the ground-state and the first two low-lying isomers for $Co_{12}Rh_{11}$ bimetallic nanoparticles. These structures form triple double-icosahedrons, characterized by three interpenetrating 19-atom double-icosahedron structures, exactly

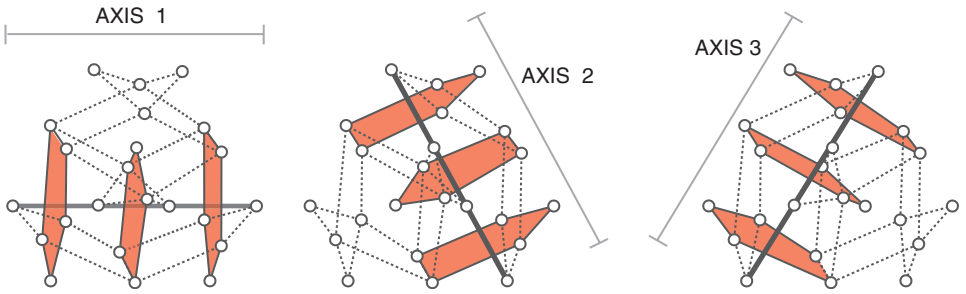

Fig. 5. (color on-line). Schematic representation of 23-atom icosahedral nanoparticle and its decomposition into double 19-atom icosahedra along the three main axes. This structure is observed in $Co_{12}Rh_{11}$ nanoparticles (cf. Fig. 4).

Table 4
Geometric characteristics of 23-atom $Co_{12}Rh_{11}$ nanoparticles

Iso	N_{Co-Co}	N_{Rh-Rh}	N_{Co-Rh}	D_{Co-Co}	D_{Rh-Rh}	D_{Co-Rh}	$\langle D\rangle$	σ
GS	21	18	48	0.896	1.001	0.964	0.955	−0.103
01	21	18	48	0.897	1.000	0.964	0.955	−0.103
02	20	17	50	0.895	1.000	0.965	0.956	−0.149

The number of bonds formed between the A and B atomic species is denoted by N_{A-B}. The associated average bond length is D_{A-B}. Total number of bonds is 87. All lengths are in units of bulk Rh–Rh bond length (2.69 Å).

as the ones we found to be the ground-state and low-lying isomers in the case of 19-atom Co–Rh nanoparticles (cf. Fig. 3). Fig. 5 schematically shows the three main icosahedral axes and their associated 19-atom double icosahedral clusters.

It is interesting to observe that $Co_{12}Rh_{11}$ bimetallic nanoparticles have their three main icosahedral axes made exclusively of Co atoms (with the exception of iso02-$Co_{12}Rh_{11}$, see Fig. 4), a characteristic shared with the 19-atom Co–Rh clusters discussed above and depicted in Fig. 3. Surface segregation of Rh atoms is not as clear for $Co_{12}Rh_{11}$ as it is for smaller nanoscale Co–Rh particles (i.e., 13-atom and 19-atom Co–Rh clusters). However, the ground-state and the low-lying isomers $Co_{12}Rh_{11}$ structures have some additional geometric peculiarities that are worth to be mentioned. First, the ground-state structure each of the three, interpenetrating double icosahedrons have the same distribution of Co and Rh, that is, a main axis composed by Co atoms, with pentagons perpendicular to such axis each having 3 Rh + 2 Co atoms, 4 Rh + 1 Co atoms, and 3 Rh + 2 Co atoms; respectively [see Fig. 4(a)]. Second, the ground-state and the first low-lying isomer are related via an inter-pentagonal atomic exchange [marked with arrows in Figs. 4(a) and (b)] between pentagons belonging to icosahedral axis 2 (cf., Fig. 5).

For the triple double-icosahedral Co–Rh nanoparticles, is difficult to visualize whether the structure has a layered or mixed atomic arrangement. The proposed order parameter σ [Eq. (4)] is helpful here to quantify the degree of ordering in each nanoparticle as a function of size. Our results for the $Co_{12}Rh_{11}$ nanoparticles confirmed the tendency observed for 19-atom and 13-atom Co–Rh bimetallic clusters in that the value of σ for the ground-state and the first isomer was the same for each size. More importantly, however, is that an inspection of the value of the order parameter reveals that Co–Rh nanoparticles become less ordered as they get bigger (cf., Tables 2–4), suggesting that large Co–Rh might be either atomically disordered ($\sigma\sim0$) or even showing a core-shell structure ($\sigma>0$). Recent tight-binding calculations on large Co_nRh_m nanoparticles ($n\sim m\sim55$), where a local geometry optimization

was performed on selected structures, showed that core-shell structures are favored over the alloyed (mixed atomic distribution) case [37], thus setting on solid grounds the trends observed in our symbiotic-algorithm fully optimized (geometry and atomic configuration) Co–Rh bimetallic clusters. Table 4 presents other geometrical properties of these triple double-icosahedral Co–Rh nanoparticles (average size ~7.9 Å).

4. Discussion

We have used a combined tight-binding and evolutionary search approach to investigate the structural and magnetic properties of Co–Rh nanoparticles. Such approach relies, on the one hand, on a suitable parametrization of the electronic Hamiltonian and, on the other, upon the appropriateness of a Gupta potential to describe the (structural) energy landscape for such alloys at the nanoscale. We have discussed the latter, to a certain extent, in Section 2.1. We now devote some space to enlarge the discussion of the former, through the direct comparison of our electronic parametrization with some published ab initio results. Fig. 6 schematically shows the equilibrium geometry, as predicted by Dennler et al., in Ref. [36], for Co_2Rh_2 bimetallic clusters.

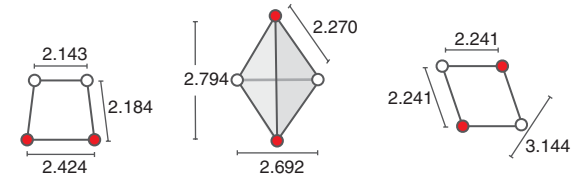

Fig. 6. (color on-line). Schematic representation of the equilibrium geometries obtained in Ref. [36] via first-principles total-energy calculations of Co_2Rh_2 nanoparticles. All interatomic distances are in angstroms. The different average values for the magnetic moment (in Bohr magnetons), as obtained from our tight-binding calculations, are reported for each bimetallic cluster. Dennler et al. [36] results are shown in parenthesis. See the text for further details.

In order for our comparison to make sense, we did not optimize the cluster geometry, but instead used the ones proposed in Ref. [36]. Below each Co_2Rh_2 cluster in Fig. 6, we have given the average magnetic moment, either decomposed by atomic species or the particle's total average.

In all cases our results for the magnetic moment followed the trends displayed by the first-principles calculations, although the tight-binding calculations systematically overestimated the magnetic moment. For the tetrahedral- and rhombohedral-shaped Co_2Rh_2 nanoparticles [Figs. 6(b) and (c), respectively] our calculations overestimate the magnetic moment by about 13%. However, for the trapezoidal-shaped Co_2Rh_2 our tight-binding parametrization showed a 31% departure from the ab initio predicted magnetic moment. One must always keep in mind, that our electronic parametrization was carried out on the basis of fitting the bulk Co magnetic moment and selected icosahedral Rh clusters (13 and 19 atoms), and that it is well known that such tight-binding parametrizations perform better as the system size increases. All things considered, we believe that, in general, our tight-binding calculations are accurate within 13% of the ab initio predicted magnetic moment.

It is inviting to relate the quantitative differences between our tight-binding and the first-principles calculations to changes in the nanoparticle bond lengths. We have analyzed this by monitoring the magnetic moment as we apply an hydrostatic distortion (uniform pressure) on Co_7Rh_6 icosahedral clusters. Fig. 7 summarizes our findings. It is interesting to observe that for the ground-state, the magnetic moment varies smoothly with bond-length and follow the expected behavior, that is, decreasing with compression and increasing with expansion (towards the atomic limit). Contrast this with the results obtained for an artificial Co_7Rh_6 nanoparticle constructed so that it displays a fully segregated configuration: the upper cap of the 13-atom icosahedron is made of Co atoms whereas the lower cap is formed of Rh atoms. The comparison of these two Co_7Rh_6 isomers brings an interesting observation concerning the sensitivity of Co and Rh to local environment effects. The averaged Co magnetic moment (squares in Fig. 7) is virtually insensitive

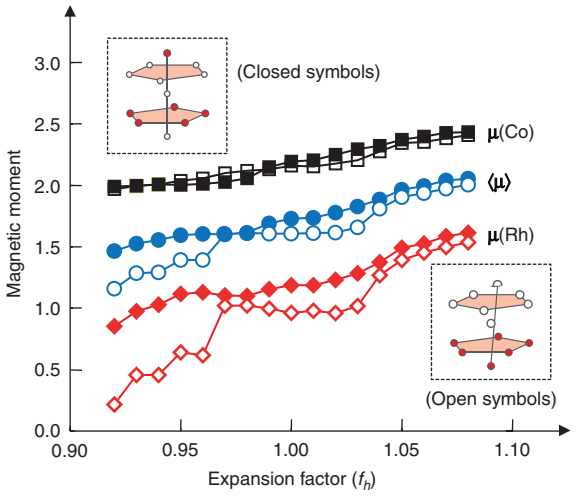

Fig. 7. (color on-line). Variation of the magnetic moment as a function of an hydrostatic distortion. The different averaged values for the magnetic moments (in Bohr magnetons) are reported in each case, e.g., μ(Co) stands for averaged value of the magnetic moment of all Co atoms. Parameter $f_h = V/V_0$ where V_0 is the equilibrium nanoparticle volume and V is the compressed ($f_h < 1.0$) or expanded ($f_h > 1$) new volume. Closed symbols stand for the Co_7Rh_6 ground-state structure while open symbols denote results for Co_7Rh_6 isomer with a "block" structure (see the insets).

to the arrangement of remaining Rh atoms. However, the Rh-averaged magnetic moment shows a strong dependency on the local environment (diamonds in Fig. 7), behaving smoothly when the cluster has an homogeneous atomic distribution, whereas showing a stepwise behavior for the segregated cluster. A similar behavior of the magnetic moment has been reported in pure Rh clusters under homogeneous deformations [21].

Regarding the effect of the chemical ordering on the properties of Co–Rh cluster, comparison between the results of Ref. [37] for large Co–Rh nanoparticles and the present findings show an important feature. Large Co–Rh nanoparticles with hundreds of atoms show that Co segregates to the surface [37], consistently with its lower surface energy, whereas for small Co_pRh_q ($p, q < 13$) the opposite trend is observed, that is, surface sites are occupied by Rh atoms. In other words, *surface segregation qualitatively and quantitatively depends on particle size for Co–Rh nanoparticles*. This is an important result, especially for catalysis applications, where it is well known that catalytic activity strongly depends on surface composition [53,54]. Our results point toward a critical cluster size that separates the Rh-segregated regime (small clusters) from the Co-segregated regime (large particles).

5. Conclusions

Bimetallic nanoparticles of Co and Rh display a variety of properties that are strongly dependent on size, composition, and structure. Surface segregation seems to have two regimes. For small Co–Rh clusters, segregation is dominated by size effects, that is, bigger atoms are located in the surface (in our case Rh), whereas for large nanoparticles, the component with lower surface energy segregates to the surface (Co atoms in our case). In fact, based on the trends observed on this, and other work on Co–Rh nanoparticles [37], there should be a critical cluster size, approximately located between 30 and 110 atoms, that separates each regime. This might have important consequences for heterogeneous catalysis, where the catalytic activity strongly depends on surface composition.

From our combined tight-binding and evolutionary search approach, we observed that the enhanced magnetism can be qualitatively related to the number of Co–Rh bonds present in the cluster and to the surface effects, particularly when Rh atoms are located at surface sites. However, even for structures having the same order (same value of σ), minute variations in the atomic configuration produce changes in the nanoparticle magnetism, that is, the magnetic properties of Co–Rh bimetallic particles are sensitive to the local environment. This fact underscores the importance of determining both the geometrical structure and the chemical configuration for heterogeneous metallic nanoparticles.

The proposed approach of combining exhaustive search of the structural energy landscape, via a symbiotic algorithm on a Gupta potential, with an unrestricted spd tight-binding Hamiltonian appears as a promising tool for investigating, at the

experimental size ranges, the structural and electronic properties of metallic alloys in the nanoscale.

Finally, the system under investigation has some resemblance to the FeCo spin glasses possessing intermediate structural order [55], where the observed conformations may be explained by the contributions of the long-range ordered spins to the electronic dipole moments. This was experimentally confirmed in Ref. [55] via the determination of the second-order nonlinear optical susceptibilities caused by the contribution of collective spin interactions.

Acknowledgements

This work was supported in part by CONACyT (Mexico) under Grant no. 40393-A and by DGAPA-UNAM project 104402. Financial support from the Spanish Ministry of Science and Technology (MCyT) Project no. MAT2002 04393 C02 01 and the Junta de Castilla-León Project no. VA 073/02 is gratefully acknowledged. F. A. -G. and J. M. M. -C. acknowledge PROMEP-SEP-CA230.

References

[1] L. Aitchison, A History of Metals, MacDonald and Evans, London, 1969.
[2] E. Hornbogen, in: R.W. Cahn, P. Haasen, (Eds.), Physical Metallurgy, third ed., North-Holland, New York, 1983.
[3] M.F. Collins, J.B. Forsyth, Philos. Mag. 8 (1963) 401.
[4] R.E. Walstedt, J.H. Wernick, Phys. Rev. Lett. 20 (1968) 856.
[5] J.L. Moran-Lopez (Ed.), Physics of Low-Dimensional Systems, Plenum, New York, 2001.
[6] J.P. Butcher, D.C. Douglass, L.A. Bloomfield, Phys. Rev. Lett. 66 (1991) 3052.
[7] D.C. Douglass, A.J. Cox, J.P. Butcher, L.A. Bloomfield, Phys. Rev. B 47 (1993) 12874.
[8] I.M.L. Billas, J.A. Becker, A. Chatelain, W.A. de Heer, Phys. Rev. Lett. 71 (1993) 4067.
[9] I.M.L. Billas, A. Chatelain, W.A. de Heer, Science 265 (1994) 1682.
[10] S.E. Apsel, J.W. Emmert, J. Deng, L.A. Bloomfield, Phys. Rev. Lett. 76 (1996) 1441.
[11] R. Galicia, Rev. Mex. Fis. 32 (1985) 51.
[12] B.V. Reddy, S.N. Khanna, B.L. Dunlap, Phys. Rev. Lett. 70 (1993) 3323.
[13] A.J. Cox, J.G. Louderback, L.A. Bloomfield, Phys. Rev. Lett. 71 (1993) 923.
[14] A.J. Cox, J.G. Louderback, S.E. Apsel, L.A. Bloomfield, Phys. Rev. B 49 (1994) 12295.
[15] V.L. Moruzzi, P.M. Marcus, Phys. Rev. B 39 (1989) 471.
[16] K. Wildberger, V.S. Stepanyuk, P. Lang, R. Zeller, P.H. Dederichs, Phys. Rev. Lett. 75 (1995) 509.
[17] V.S. Stepanyuk, W. Hergert, P. Rennert, K. Wildberger, R. Zeller, P.H. Dederichs, Phys. Rev. B 54 (1996) 14121.
[18] Y. Jinlong, F. Toigo, W. Kelin, Phys. Rev. B 50 (1994) 7915.
[19] P. Villaseñor-Gonzalez, J. Dorantes-Davila, H. Dreysse, G. Pastor, Phys. Rev. B 55 (1997) 15084.
[20] M. Moseler, H. Hakkinen, R.N. Barnett, U. Landman, Phys. Rev. Lett. 86 (2001) 2545.
[21] E.O. Berlanga-Ramírez, F. Aguilera-Granja, A. Díaz-Ortiz, A. Vega, European Phys. J. D 23 (2003) 343.
[22] E.O. Berlanga-Ramírez, F. Aguilera-Granja, A. Díaz-Ortiz, J.L. Rodríguez-López, A. Vega, Phys. Lett. A 318 (2003) 473.
[23] D.I. Bazhanov, W. Hergert, V.S. Stepanyuk, A.A. Katsnelson, K. Kokko, C. Demangeat, Phys. Rev. B 62 (2000) 6415.
[24] A. Delin, E. Tosatti, R. Weht, Phys. Rev. Lett. 92 (2004) 057201.
[25] For a recent review see N. Toshima, T. Yonezawa, New J. Chem. 21 (1998) 1179.
[26] T. Ould Ely, C. Amiens, B. Chaudret, E. Snoeck, M. Verelst, M. Respaud, J.-M. Broto, Chem. Mater. 11 (1999) 526.
[27] J. Osuna, D. de Caro, C. Amiens, B. Chaudret, E. Snoeck, M. Respaud, J.-M. Broto, A. Fert, J. Phys. Chem. 100 (1996) 14751.
[28] F. Dassenoy, K. Philippot, T. Ould Ely, C. Amiens, P. Lecante, E. Snoeck, A. Mosset, M.-J. Casanove, B. Chaudret, New J. Chem. 22 (1998) 703.
[29] M. Respaud, J.M. Broto, H. Rakoto, A.R. Fert, L. Thomas, B. Barbara, M. Verelst, E. Snoeck, P. Lecante, A. Mosset, J. Osuna, T. Ould Ely, C. Amiens, B. Chaudret, Phys. Rev. B 57 (1998) 2925.
[30] T. Ould Ely, C. Pan, C. Amiens, B. Chaudret, F. Dassenoy, P. Lecante, M.-J. Casanove, A. Moset, M. Respaaud, J.-M. Broto, J. Phys. Chem B 104 (2000) 695.
[31] D. Zitoun, C. Amiens, B. Chaudret, M. Respaud, M.-C. Fromen, P. Lecante, M.-J. Casanove, New J. Phys. 4 (2002) 77.
[32] D. Zitoun, M. Respaud, M.-C. Fromen, M.-J. Casanove, P. Lecante, C. Amiens, B. Chaudret, Phys. Rev. Lett. 89 (2002) 037203.
[33] D. Zitoun, C. Amiens, B. Chaudret, M.-C. Fromen, P. Lecante, M.-J. Casanove, M. Respaud, J. Phys. Chem. B 107 (2003) 6997.
[34] Experiments consider that all spin polarization is localized on Co sites. Thus, this value corresponds to the magnetization per CoRh unit.

[35] G. Moraitis, H. Dreysee, M.A. Khan, Phys. Rev. B 54 (1996) 7140.
[36] S. Dennler, J. Morillo, G.M. Pastor, Surf. Sci. 532–535 (2003) 334.
[37] E.O. Berlanga-Ramírez, F. Aguilera-Granja, J.M. Montejano-Carrizales, A. Díaz-Ortiz, K. Michaelian, A. Vega, Phys. Rev. B 70 (2004) 014410.
[38] D.E. Goldberg, Genetic Algorithms in Search Optimization and Machine Learning, Addison-Wesley, Reading, MA, 1989.
[39] S. Forrest, Science 261 (1993) 872.
[40] D.M. Deaven, K.M. Ho, Phys. Rev. Lett. 75 (1995) 288.
[41] M.D. Wolf, U. Landman, J. Chem. A 102 (1998) 6129.
[42] K. Michaelian, N. Rendón, I.L. Garzón, Phys. Rev. B 60 (1999) 2000.
[43] R. Poteau, G.M. Pastor, Eur. Phys. J. D 9 (1999) 235.
[44] K. Michaelian, Chem. Phys. Lett. 293 (1998) 202.
[45] R.P. Gupta, Phys. Rev. B 23 (1981) 6265.
[46] F. Cleri, V. Rosato, Phys. Rev. B 48 (1993) 22.
[47] D.A. Papaconstantopoulos, Handbook of the Band Structure of Elemental Solids, Plenum, New York, 1986.
[48] R. Haydock, in: E. Ehrenreich, F. Seitz, D. Turnbull, (Eds.), Solid State Physics, vol. 35, Academic Press, London, 1980, p. 215.
[49] C. Kittel, Introduction to Solid State Physics, seventh ed., Wiley, New York, 1996.
[50] J.L. Rodríguez-López, F. Aguilera-Granja, K. Michaelian, A. Vega, Phys. Rev. B 67 (2003) 174413.
[51] F. Ducastelle, Order and Phase Stability in Alloys, in: F.R. de Boer, D.G. Petiffor, (Eds.), Cohesion and Structure, vol. 3, North-Holland, Amsterdam, 1991.
[52] The second isomer (iso02) for $Co_{10}Rh_9$ is also related to the ground-state structure through a rotation of $2\pi/5$ (clockwise) around the main icosahedral axis. This property is not present in the second low-lying isomer of Co_9Rh_{10}.
[53] J.H. Sinfelt, Bimetallic Catalysis, Wiley, New York, 1985.
[54] V. Ponec, G.C. Bond, Catalysis by Metals and Alloys, Elsevier, Amsterdam, 1995.
[55] W. Gruhn, I.V. Kityk, S. Benet, Mater. Lett. 55 (2002) 158.